Chirality on Dendrimers: "Roll Booster" of the Molecule-level Self-sorting Assembly in Two-component Supramolecular Gel System†

(Supporting information)

Huiwen He[†§], Hao Zheng[†], Meng Ma[†], Yanqing Shi[†], Zengliang Gao[§], Si Chen[†*], Xu Wang[†*]

[†]College of Materials Science and Engineering, Zhejiang University of Technology, 18 Chaowang Road, Hangzhou 310014, China.

[§]College of mechanical and Engineering, Zhejiang University of Technology, 288 Liuhe Road, Hangzhou 310000, China.

1. Materials and methods

All materials employed in the paper were commercially available. Octa (3-aminopropyl) silsesquioxanes hydrochloride (Octa-Ammonium POSS-OAS) was purchased from hybrid plastic (Hattiesburg, MS). N,N,N,N'-Tetram-ethyl-O-(1H-benzotriazol-1-yl)uroniumhexafluorophosphate (HBTU), 1-hydroxybenzotriazole(HOBt), HATU, Boc-6-Ahx-OH, N-Methylmorpholine (NMM) and Boc-DL-Lys(Boc)-OH were supplied by Aladdin (Shanghai, China) and used as received. All solvents used in the synthesis were analytical pure and used without further purification. Silica column chromatography was carried out using silica gel (200-300 mesh) provided by Qingdao Haiyang Chemical (Qingdao, China). Thin layer chromatography was performed on commercially available glass backed silica plates.

Gelation ability and gel-sol transition temperature (T_{gel}). For the gelation test, a known weight (20 mg) of a tested compound and a measured volume (1 mL) of a chosen liquid were placed into a 3 mL glass vial as a test tube. During the test, the system was ultrasonic treated for 5 min at room temperature, then the test tube was heated until the solid was dissolved completely, after that the system was cooled to room temperature. Finally, the test tube was inversed to observe the state of the materials inside. The *Tgel* was measured by using a simple tube-inversion method. We defined the temperature at which the gels began to flow the gel-sol transition temperature as the gel point.

Field emission scanning electron microscopy (FESEM). The samples were carefully scooped onto the silicon wafer with a clean surface and allowed to dry overnight in the air. Vacuum drying was carried out in vacuum room temperature for 8 h to remove the solvent trapped in gel networks. Then 10 nm-thick platinum films were deposited on the gels. Finally, the morphology of the gels was investigated by using a Hitachi S-4700 FESEM operated at 15 kV.

Transmission electron microscopy (TEM). For the gel, the material as a sol was drop coated on amorphous carbon-coated Cu grids. In both cases, the concentration of the gelators were below the minimum gelator concentration, due to the resultant aggregates were too thick to get good-quality micrograph at higher concentrations. TEM images were recorded by using a JEM-1230

microscope at an accelerating voltage of 80 kV.

Wide angle X-ray diffraction (XRD). The diffraction patterns were obtained using a Shimadzu XRD-6000 diffractometer with a Ni filter and CuKα (l = 1.54056 Å, voltage = 40 kV, and cur-rent = 40 mA). Each sample was scanned over the range from 1 °C to 40 °C with a sweep speed 5 °C·min^{-1}.

Rheology. Rheological characterizations of gels were per-formed on an Anton Paar MCR302 Rheometer with plate geometry (PP 25). The gap distance between plate and plate was fixed at 0.2 mm. Rheological measurements were carried out on freshly prepared gels and were scooped onto the plate of the Rheometer. The following tests were performed: the samples were submitted to this parallel-plate very quickly to minimize solvent evaporation. Dynamic strain sweep tests were increased amplitude of oscillation from 0.1 % up to 100 % apparent strain shear (kept a frequency ω=10 rad·s^{-1}) at 25 °C. Dynamic frequency sweep tests were between 0.1 and 100 rad·s^{-1} (kept a strain γ=0.1 %) at 25 °C, oscillatory frequency sweep experiments were performed in the linear viscoelastic region to ensure calculated parameters correspond to an intact network structure.

2. Synthesis and characterization

Synthesis of G1: G1 was synthesized as same as the literature reported before in our group[1].

Synthesis of G1(R): racemic lysine-containing dendrimer **G1(R)** was synthesized as same as the **G1** with only $_L$-lysine have been replaced by the racemic lysine. The structure of **G1(R)** is shown as below. Yield 88.0%. ^{1}H NMR (DMSO-d6, 500 MHz, ppm), 7.74 (8H, s, $CH_2NHCOCH_2$), 6.70 (8H, t, CHN*H*-Boc), 6.38 (8H, t, CH_2NH-Boc), 3.79 (8H, t, C*H*(CH_2)NHCO), 3.06 (32H, t, CH_2CH_2NH-Boc), 2.82 (16H, t, CH(CH_2)NHCO), 1.54-1.29 (48H, m, $CH_2CH_2CH_2$), 1.40-1.25 (144H, m, CH_3), 0.52 (16H, t, SiCH_2). ESI/APCI-MS: The calculated $[M+Na]^{2+}/2$ of **G1(R)** was 1776.5 and the test result was 1776.9, results fit with the calculation.

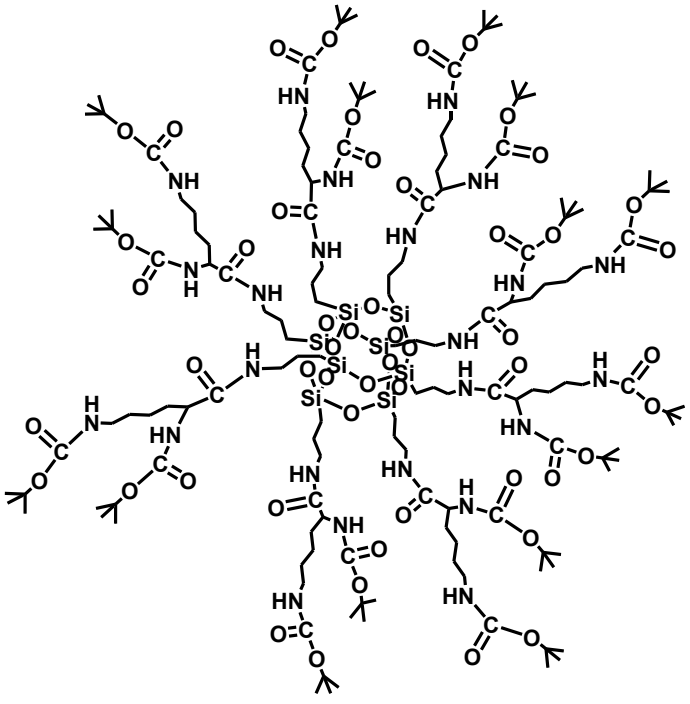

Figure S1. The chemical structure of **G1(R)**.

Synthesis of G2: Lys(G2)-OH(2.7 g, 3.36 mmol, the synthetic methods has been reported by D.K Smith[2]), NMM(0.7 g, 6.93 mmol) and HATU(1.28 g, 3.36 mmol) were dissolved in DMF (20 mL) and the mixture was stirred for 5min to make the condensing agent activated. Then Octa Ammonium POSS (0.31 g, 0.26 mmol) were added to the solution. The mixture was reacted under strong stirring for 24 h at 25 ^{o}C. After the reaction, the white turbid solution was obtained. Distilled water (100mL) was added to the turbid solution and then a mass of white solid was precipitated. After purified by silica column chromatography (CH_2Cl_2/CH_3OH= 10/1, Rf=0.65), the target product was obtained as fine white solid. Yield=75 %. ^{1}H NMR δH ($CDCl_3$, 500 MHz, ppm) 7.68-7.43 (24H, br, CH_2N*H*CO), 6.03-5.81 (16H, br, CH_2N*H*BOC), 5.20-4.98 (16H, br, CHN*H*BOC), 4.45-4.03 (24H, brm, COCH(R)NH), 3.18-3.09 (64H, brm, CH_2N*H*), 1.91-1.27 (448H, m, C*H*$_2$, C*H*$_3$), 0.61(16H, s, Si*CH*$_2$). ESI-MS: Calculated for G2 $[M+3Na]^{3+}/3$=2409.75, test result was 2409.1; $[M+4Na]^{4+}/4$=1812.06, test result was 1812.1; $[M+5Na]^{5+}/5$=1455.05, test result was 1453.6; results fit with the calculation.

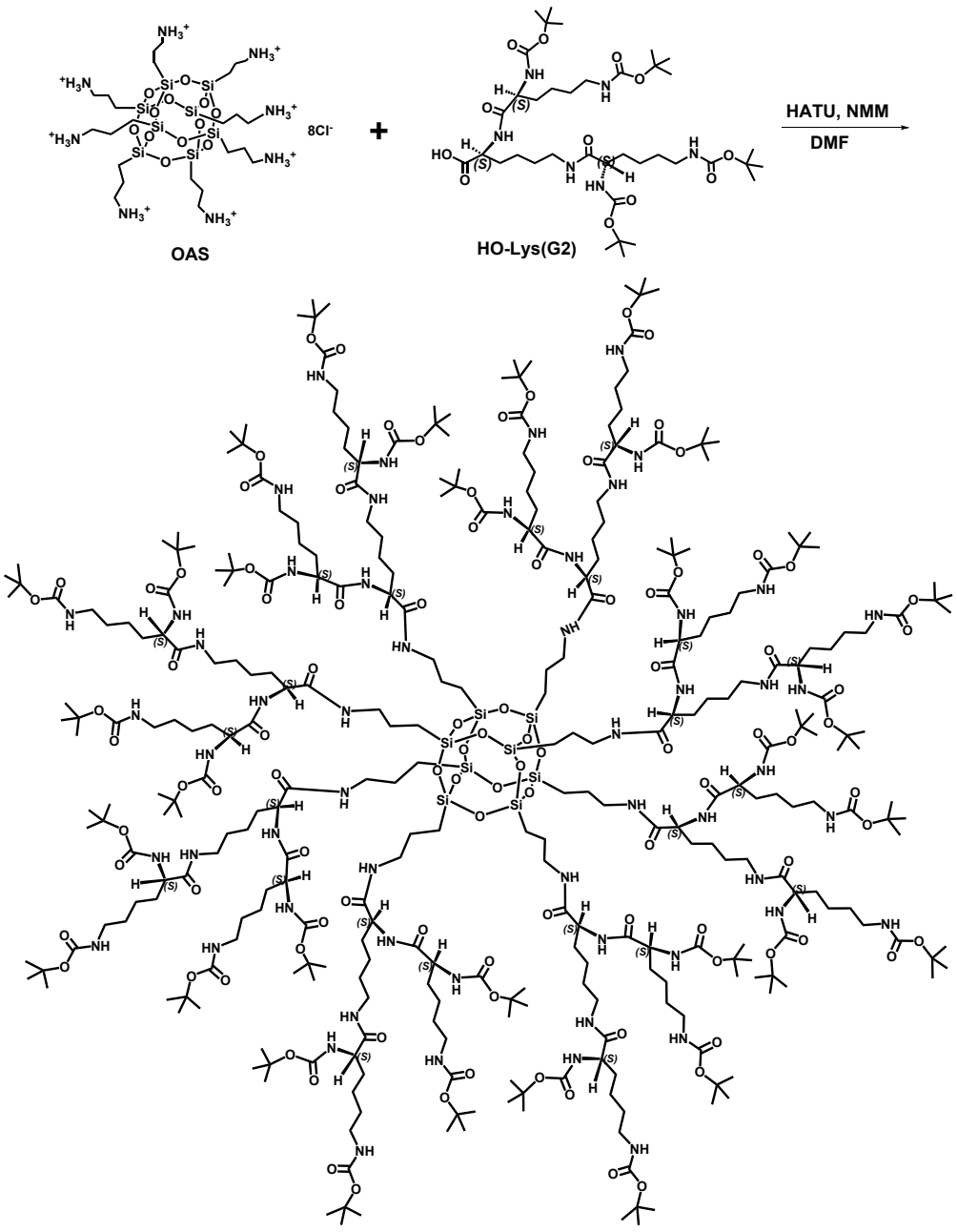

Scheme S1. The synthesis route for **G2**.

Synthesis of C6: Boc-6-Ahx-OH (4.62 g, 20 mmol), HBTU (7.61 g, 5 mmol) and HOBt (2.98 g, 22 mmol) were dissolved in DMF (30 mL) and the mixture was stirred in 100 mL round bottom flask for 5min to make the condensing agent activated. Then Octa Ammonium POSS (2.34 g, 2 mmol) and NMM (36 mmol, 3.64 g) were added to the solution. The mixture was reacted under strong stirring for 24 h at 25 ^{o}C. After the reaction, the green turbid solution was obtained. Distilled water (200mL) was added to the turbid solution and then a mass of white solid was precipitated. The produced white solid was separated by centrifugation (10000 r/min, 10 min) and the obtained white crude product was washed by acetonitrile for 3 times. After purified by silica column chromatography (CH_2Cl_2/CH_3OH= 9/1, Rf=0.65), the target product was obtained as fine white solid. Yield=61%. ^{1}H NMR (DMSO-d_6, 500 MHz, ppm), 7.77 (8H, d, $CH_2NHCOCH_2$), 6.76 (8H,

t, N*H*-Boc), 3.01 (16H, d, CH_2CH_2NHCO), 2.88 (16H, d, CH_2CH_2NH-Boc), 2.04 (16H, t, $NHCOCH_2CH_2$), 1.54-1.39 (32H, m, $CH_2CH_2CH_2$), 1.27-1.39 (96H, m, CH_3), 1.20(16H, m, $CH_2CH_2CH_2$), 0.59 (16H, s, $SiCH_2$). FT-IR (KBr): ν=3303, 2925, 2861, 1680, 1533, 1465, 1090. ESI/APCI-TOF-MS: Calculated for **C6** $[M+2Na]^{2+}/2$ = 1316.7, and test result was 1316.7, results fit with the calculation. The elemental analyses obtained from Energy Dispersive X-ray Detector are: C, 59.34; N, 10.69; O, 24.28; Si, 5.69. The results fit with the calculated data: C, 56.76; N, 9.46; O, 24.32; Si, 9.46.

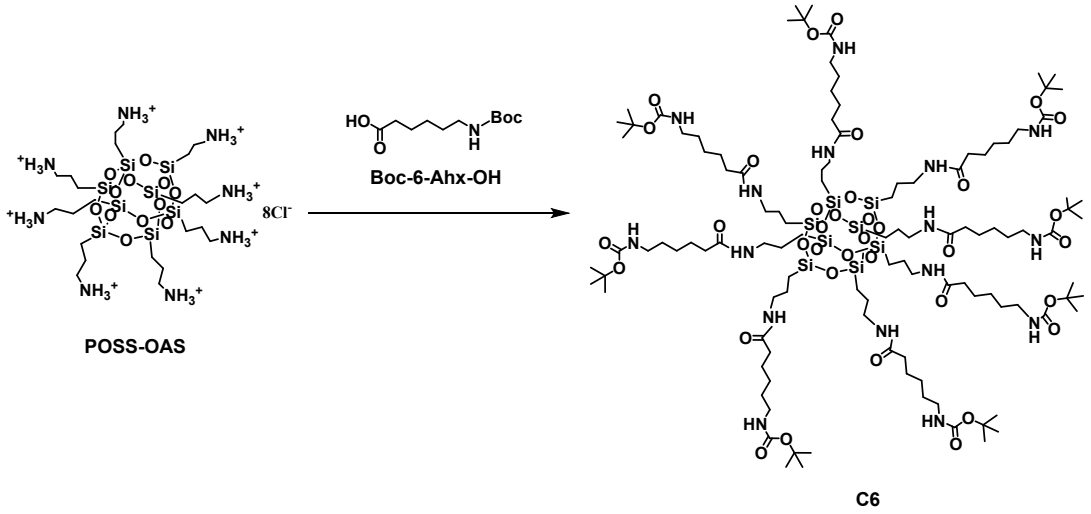

Scheme S2. The synthesis route for **C6**.

3. Independent gelation ability study of C6, G1 and G2

The gelation ability including gelling property, driving force for gelation, thermal stability and molecular packing model have been studied systematically. Unsurprisingly, lack of one amide bond in each arm structure of dendrimer, the gelling ability of **C6** seems to be much weaker as no gels formed without the acceleration of ultrasound (Table S1, Figure S2). While, **G2** shows no gelation in tested solvents.

Table S1. Gelation ability of C6 and G1 in different solvents[a]

Solvents	Polarity Index	**C6**	**G1**	**G2**
N-hexane	0.06	P	P	P
Cyclohexane	0.10	P	P	P
Toluene	2.40	TG (16)*	TG (4)	S
Chlorobenzene	2.70	TG (16)*	TG (6)	S
O-xylene	2.50	OG (8)	TG (4)	S
Styrene	3.00	OG (16)*	TG (5)	S
MMA	2.50	OG (9)*	TG (5)	S
Ethyl acetate	4.40	OG (5)*	TG (5)	S
Butyl acetate	3.90	OG (14)*	TG (5)	S
Acetone	5.10	S	TG (4)	S
THF	4.00	S	S	S
DMSO	7.20	S	S	S
DMF	6.40	S	S	S
Ethyl alcohol	5.20	S	S	S
Methanol	5.10	S	S	S

[a]P = precipitate, TG = transparent gel, OG = Opaque gel, S = solution. The data in brackets represents the minimal gel concentration (MGC), mg/mL. * represent the gelling process need the assist of ultrasound.

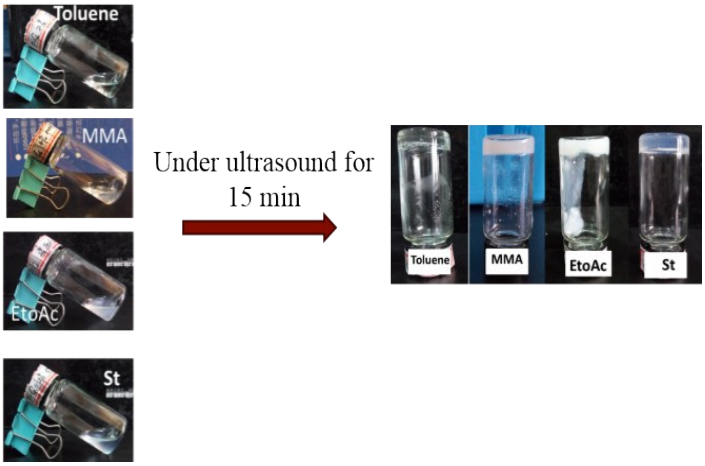

Figure S2. The digital photograph of **C6** gel formation under ultrasound for 15 min in room temperature. After the heating, melting and cooling process of **C6** in solvent, there are still only sol exist in toluene, MMA, EtoAc and styrene. After ultrasound trectment for 15 min, the gel formed.

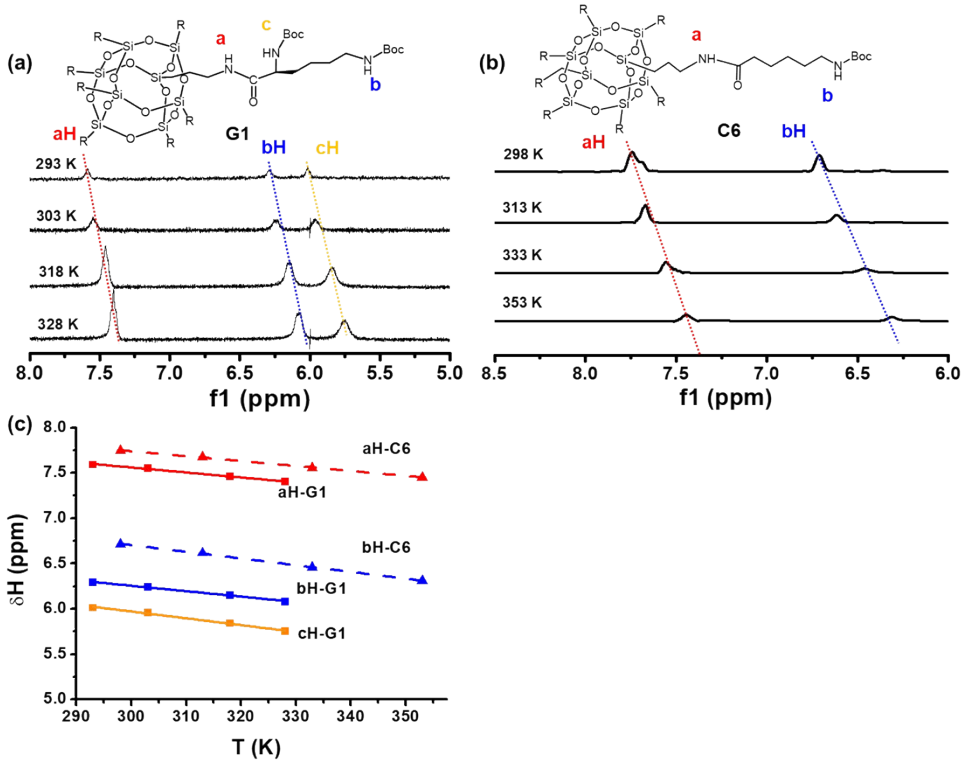

Figure S3. Variable temperature ^{1}H NMR (DMSO-d_6) of **G1** (a) and **C6** (b). (c) The linear fitting of the correspondent shifts for **G1** and **C6.** The concentration of **G1** and **C6** are in 10 mg/mL. As the temperature increases, the chemical shift of proton H on the amide bond in the **G1** and **C6** gelator gradually shifts to a high field, thus, the main driving force of gelation for **C6** is the hydrogen bonds as same as the **G1**. Furthermore, the slope of the fitting line is the same, which infer that the energy of the hydrogen bonds is the same.

The main driving force of gelation for **C6** and **G1** are the same hydrogen bonds which have been proved by variable temperature ^{1}H NMR (Figure S3), it is unusual for the structure similar dendritic gelators exhibit such an obvious difference in ultrasound induced assembly behavior. In order to describe the difference clearly, the MGC of amide bond (MGC-AB) in different solvents for **C6** and **G1** are calculated as shown in Figure S4a and Table S2. Depending on the saturation of hydrogen bond, the MGC-AB value could reflect the hydrogen bond energy directly, with higher MGC-AB represent the lower bonding strength of dendrimers. The value of MGC-AB in **C6** are much higher than in **G1**, which indicated that **C6** has a less efficient self-assembly due to the scattered stacking between dendrimers affect from weaker hydrogen bond interaction. It cannot be ignored that **G1** have eight chiral arm structure, such an architectural feature promoted the unique supramolecular chiral assembly with high thermal stability in **G1** which have been confirmed by CD spectrum in variable temperature (Figure S5). Hence, the chiral spatial feature act as the accelerant in efficient non-covalent hydrogen bonding.

The gel-sol phase transition temperature (T_{gel}) of **C6** as shown in Figure S4b which represent the thermostability of gels have also support the stronger combination of **G1** dendrimers. For **G1** gels, the T_{gel} almost achieve to 82 ^{o}C with the concentration of gelators in 60 mg/mL, a value larger than 51 ^{o}C for **C6** in saturation concentration. The big difference of T_{gel} for **C6** and **G1** is clearly shows the surprising thermal stability of the **G1** gels, which further confirm the tight packing of building blocks or well-aligned fiber networks.

Table S2. The molar amount of amide bond of gel in G1 and C6 in different solvents

Solvents	**C6**	[a]$n_{(\text{-NH-CO-})}$(μmol)	**G1**	$n_{(\text{-NH-CO-})}$ (μmol)
Toluene	TG (16)*	99.2	TG (4)	27.2
Chlorobenzene	TG (16)*	99.2	TG (6)	40.8
O-xylene	OG (8)	49.6	TG (4)	27.2
Styrene	OG (16)*	99.2	TG (5)	34
MMA	OG (9)*	55.8	TG (5)	34
Ethylacetate	OG (5)*	31	TG (5)	34
Butylacetate	OG (14)*	86.8	TG (5)	34
Acetone	S	S	TG (4)	27.2

[a] $n_{(\text{-NH-CO-})} = MGC/M_{(gelator)} * N$. $M_{(gelator)}$ is the molar mass, N is the number of amide bonds per dendrimer.

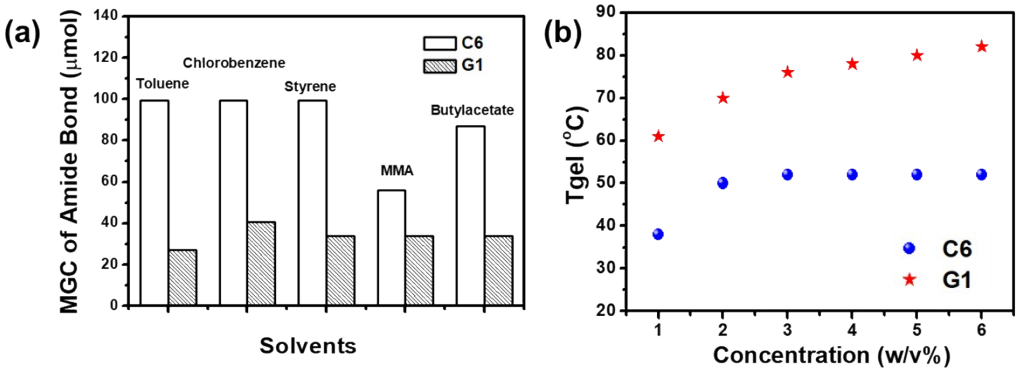

Figure S4. (a) The minimal gel concentration (MGC) of amide bond obtained from the gelation ability test of **C6** and **G1** in different solvents. (b) The phase diagram of **C6** and **G1** are obtained from methyl methacrylate (MMA) with the ultrasonication during the gel preparation process.

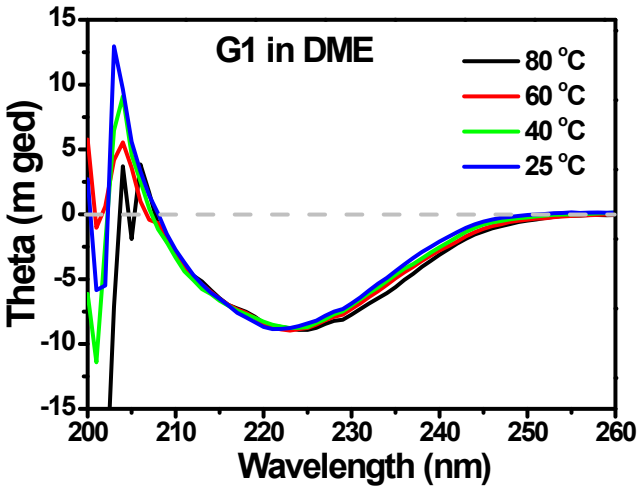

Figure S5. Variable temperature dependent Circular dichroism (CD) spectra of **G1** in DiMethyl Ether (DME) solution (The concentration is $2x10^{-7}$mol/L). As the temperature gradually increase to 80 °C, the absolute CD value shows no decreases with negative cotton effect maintained at -8 mged and absorption peak at 223 nm. Hence, a high thermal stability for chiral assembly of **G1** have been confirmed.

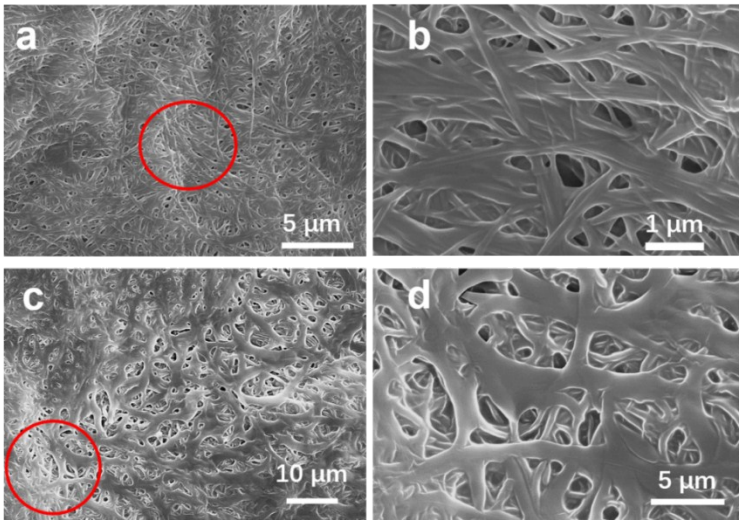

Figure S6. The SEM images of hybrid xerogel, **C6** and **G1** are in equimolar obtained from MMA, the concentration of mixed gelators in 5 mg/mL. (a) (c) are images in different field of vision, (b)(d) are the enlarge of (a) and (c). The mixed gel in MMA proved the same self-sorting assembly with two kind of fibers coexist in the same field of vision, obvious individual fiber networks bring from **C6** and **G1**.

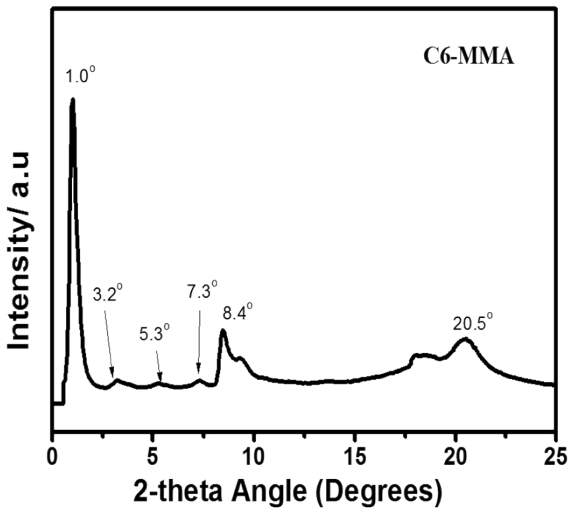

Figure S7. XRD pattern of the **C6** xerogel obtained from MMA (30 mg/mL).

XRD test was carried out to investigated the molecular packing model (Figure S6, S7). The XRD pattern of the **C6** xerogel obtained from MMA showed a distinct peak at low angle (2θ=1.02°) corresponding to d=8.80 nm. Along with relatively less intense scattering peaks at 2θ= 3.2, 5.3, 7.3, 8.4, corresponding to d= 2.76, 1.70, 1.29 and 1.05 nm, respectively, form a ratio of 1:1/√3:1/2:1/√7, a feature that strongly suggests a hexagonal columnar structure. A peak in the wide-angle region (2θ=20.5°) corresponding to the plane-to-plane stacking mode of cubic structure of the POSS core distance (d=0.43 nm). During to the hexagonal columnar structure stacking mode, 2θ=1.02° corresponding to 8.80 nm crystal distance as Figure S7 shows, which can easily be deduce the diameter of single column was 3.20 nm. Considering the molecular dimensions of the full extended length of **C6** is 3.29 nm, it was most likely that the single column was formed by stacking **C6** with a plane-to-plane model, where cubic POSS cages were fixed in the middle of a column with arms stretched outwards (Figure S7). These single columns aggregate to form a hexagonal columnar structure so as to achieve the thermodynamically stable state as **G1**.

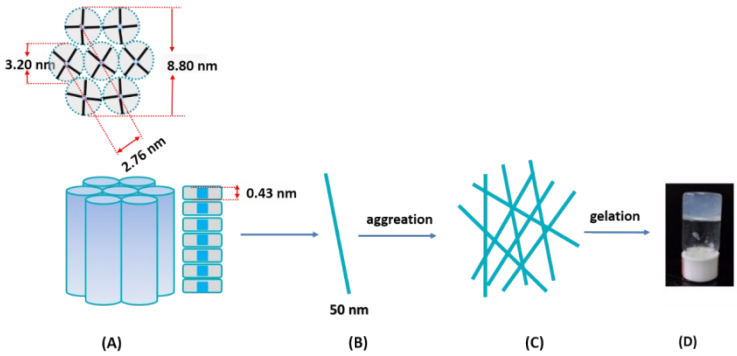

Figure S8. The self-assembly model of **C6** in MMA. (a) the molecular packing model of **C6**. (b) the assembled single fiber from **C6**. (C) the cross-overed fiber networks assembled from **C6**. (d) the digetal images of **C6** gel in a 3 mL vial (MMA as the solvent, 30 mg/mL).

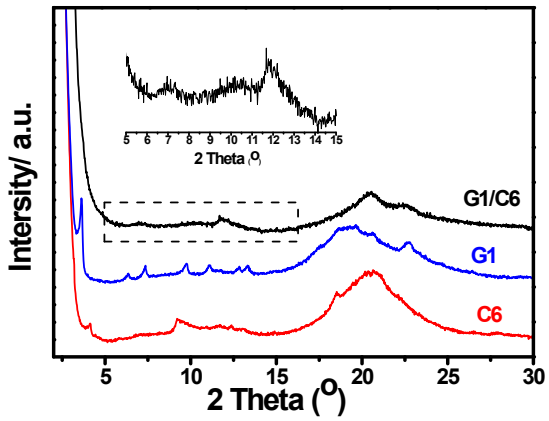

Figure S9. The XRD analysis of **C6**, **G1** and **G1**/**C6** gelators obtained from MMA (30 mg/mL).

4. Chirality recognition induced self-sorting assembly in dendritic mixed system

In order to conform the role of "chiral recognition" in self-sorting, we synthesize the racemic lysine-contained dendrimer ***G1(R)*** (Fig. 5) and dendrimer **G2** with much more chiral centers and amide groups and for the controlled experiment. Several simple but effective methods to test the self-sorting assembly have applied for **C6+G1(R)** and **C6+G2**.

From the digital images, TEM images and CD spectra of hybrid systems, no obvious self-sorting existed in complex system. Instead, the co-assembly seems to be happened. As shown in Figure. S10, both ***C6*** and ***G1(R)*** have no Cotton effect with any absorption peaks in the CD spectra, which fit the racemic nature of dendrimers. However, the complex system with ***C6*** and ***G1(R)*** in a 1:1 ratio shows a different performance, some weak absorptions appeared at around 220 nm and 330 nm which indicated the perturbation of the assembly of ***G1(R)*** by ***C6*** and shows some probable supramolecular chiral assembly. The CD results proved a molecule-level or supramolecule-level co-assembly exist in the complex system, which also can be confirmed by a transparency change in gels as shown in the inset figure in Figure. S10. The gel of ***G1(R)*** in MMA is transparent and **C6** is opaque, while, the hybrid gel **G1(R)+C6** shows a transparent feature, which different from **C6** represent the uniform fiber network formed. The TEM images of assemblies from racemic dendrimer (Fig. 6a, 6c) indicates the "loofah-like" fiber networks are absent from the tested solvents (Figure S11a, 11c), which shows no unique chiral recognition in the self-assembly of dendrimers. What's more, the TEM images of **G1(R)+C6** in MMA and toluene (Figure S11b, 11d) support the results obtained from CD spectra that there have no obvious self-sorting assembly appeared, with only one kind of fiber networks exist. Furthermore, a helix fiber appeared in Figure S11b shows the chiral assembly, confirm the CD signal. Therefore, these results intensively support that the "chiral recognition" is the key role in self-sorting self-assembly.

In **C6+G2** system, G2 shows no gelation ability in commonly used solvents might due to the too large peripheral groups, and with only random aggregations formed in solvents (Figure S12c, 12d). After study the self-sorting assembly behaviors, we found that C6 still formed nanofibers in two component assemblies. Hence, from the TEM images we can conclude that G2 and C6 shows an obviously self-sorting assembly (Figure S12a, 12b). The CD results also indicated that C6 and G2 have no co-assembly in molecule-level with no CD signal shift in absorption position and half the ellipticity of CD signals with the dilution of chiral component. Therefore, these results intensely proved that the chirality is the key for self-sorting.

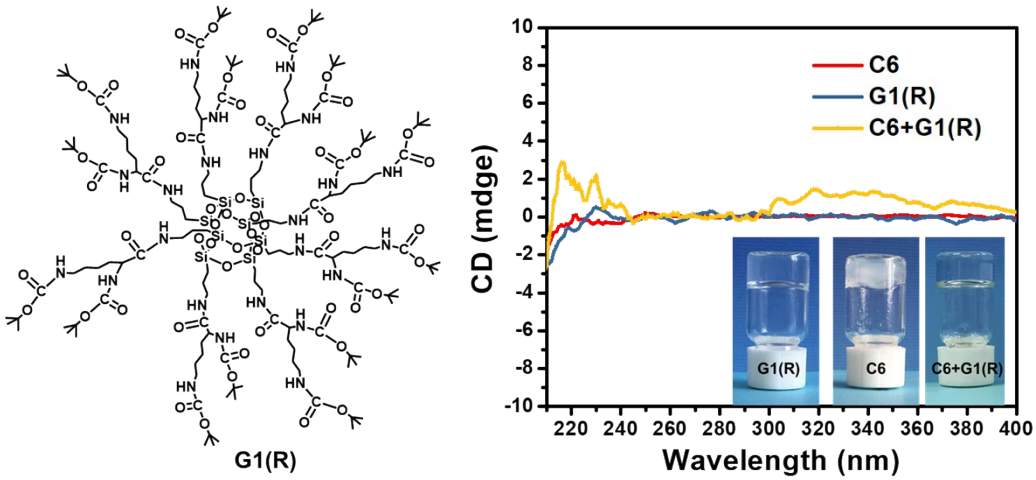

Figure S10. The chemical structure of racemic dendrimer **G1(R)** and the CD spectra of complex system in DME. The inset figures are the gel of **G1(R), C6** and **G1+C6** in MMA with a concentration in 30 mg/mL.

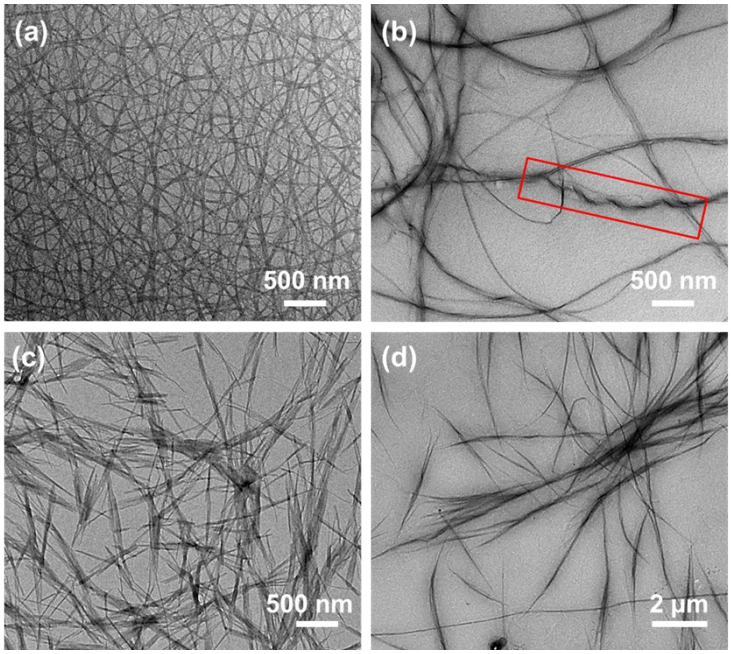

Figure S11. The TEM images of **G1(R)** and the hybrid **G1(R)+C6** xerogel in MMA and toluene. (a), (c) are the **G1(R)** in MMA and toluene. (b), (d) are the **G1(R):C6=1:1** in MMA and toluene. The concentration of gelators are in 5 mg/mL.

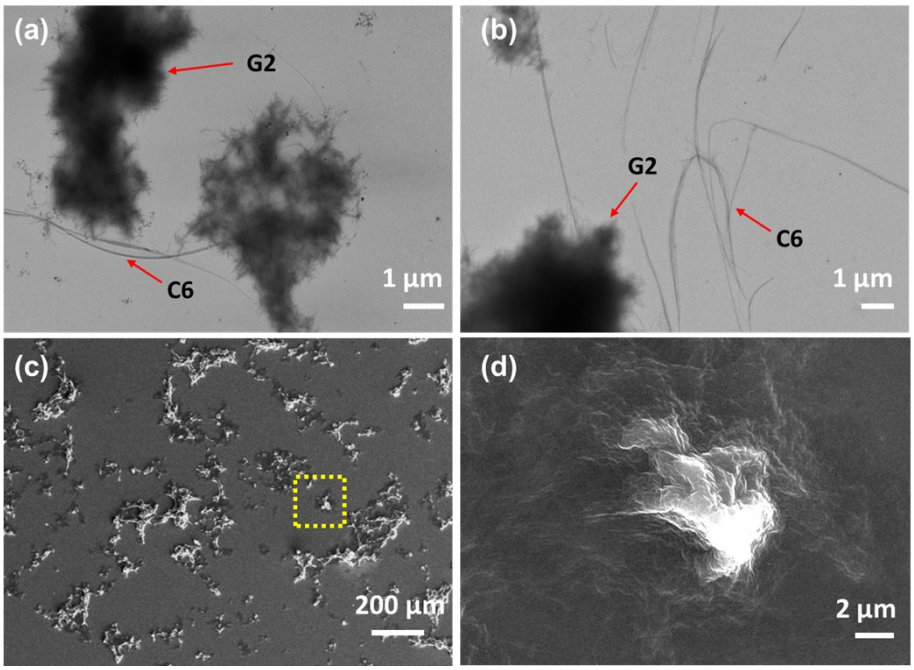

Figure S12. (a), (b) are the TEM images of **G2+C6** xerogel obtained from MMA, n(**G2**) : n(**C6**)=1:1. (c), (d) are the SEM of the dried solution of G2. The concentrations of dendrimers are in 5 mg/mL.

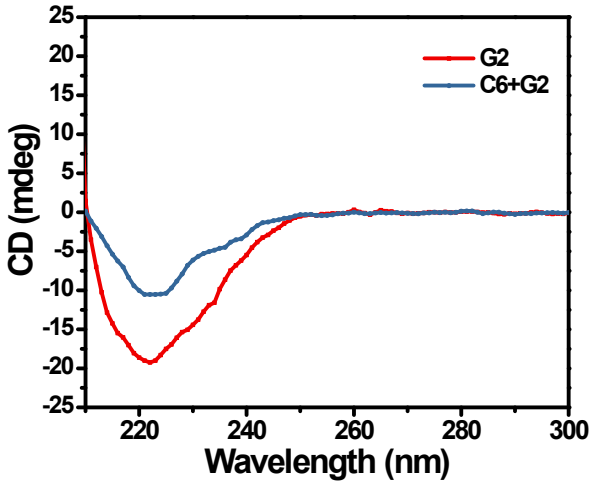

Figure S13. The CD spectra of **G2+C6** obtained from the solution of 1,2-Dimethoxyethane (DME) with a concentration in 0.6 mg/mL.

5. Characterization details

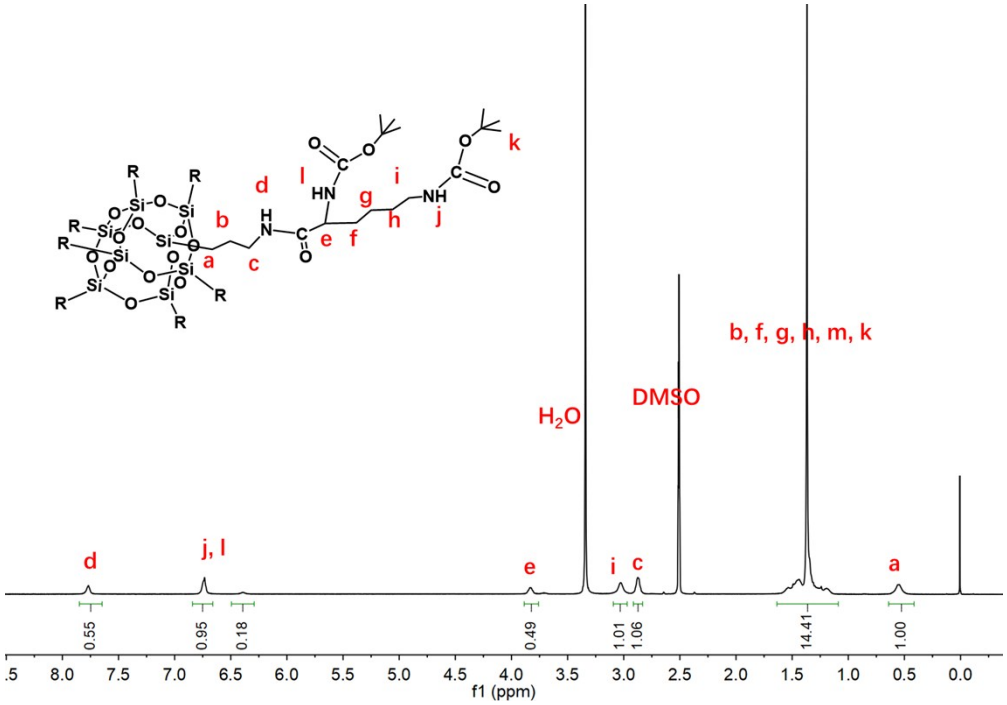

Figure S14. The ^{1}H NMR spectra of **G1(R)** in DMSO-d_6.

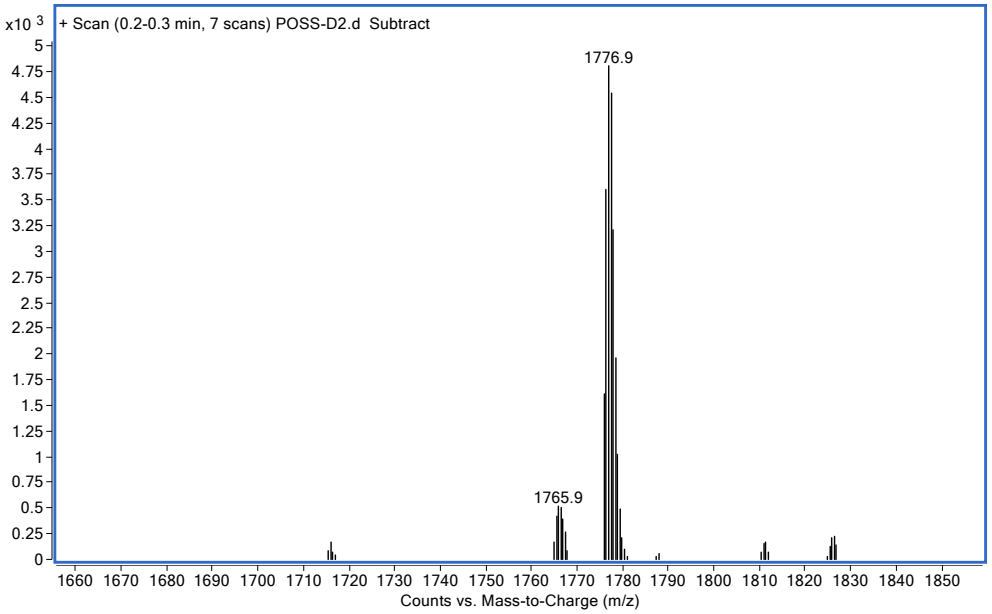

Figure S15. ESI/APCI-TOF-MS of racemized dendrimer **G1(R).**

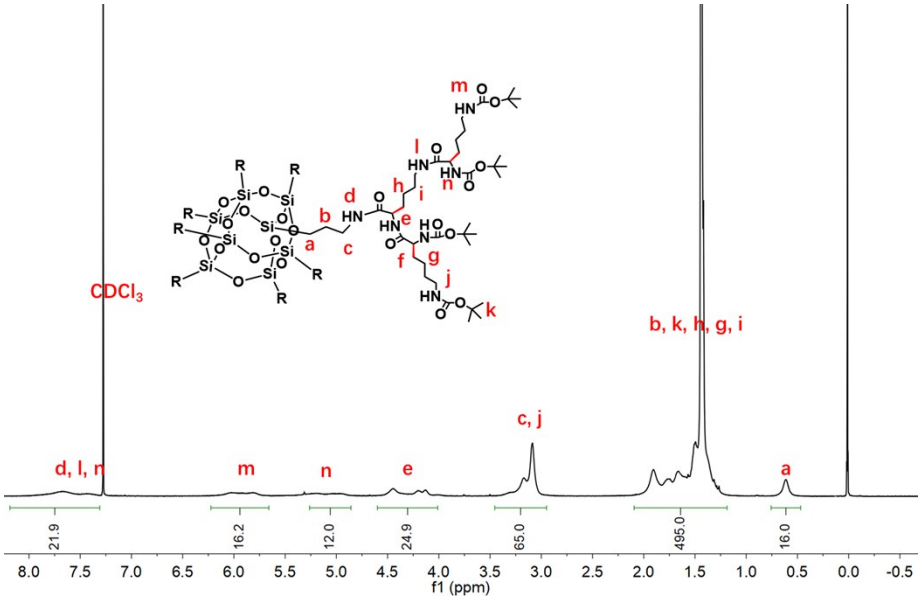

Figure S16. The ^{1}H NMR spectra of **G2** in $CDCl_3$.

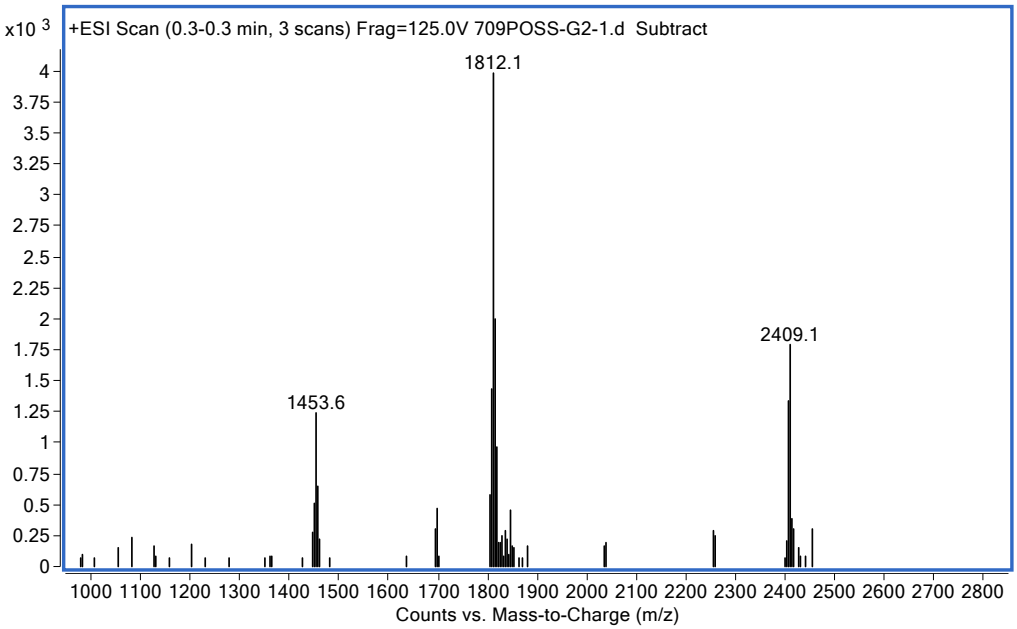

Figure S17. ESI/APCI-TOF-MS of racemized dendrimer **G2.**

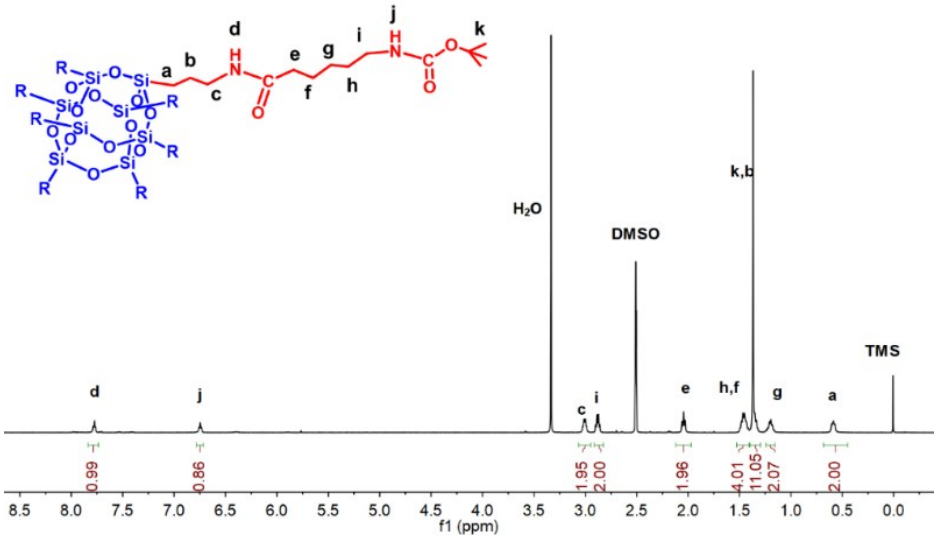

Figure S1. The ^{1}H NMR spectra of **C6** in DMSO-d_6.

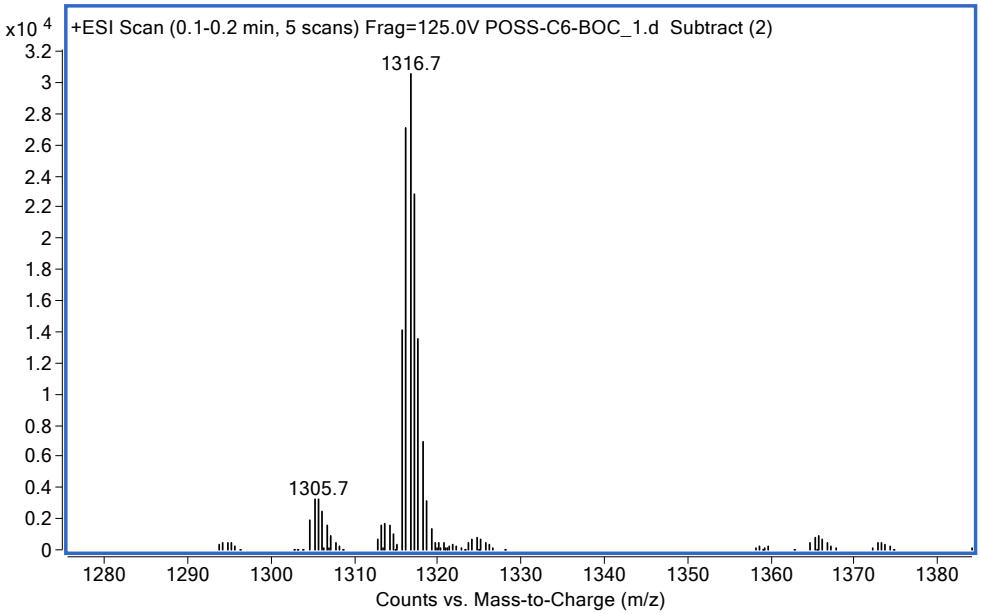

Figure S19. The ^{1}H NMR spectra of **C6** in DMSO-d_6.

References

1. G. Tang, S. Chen, F. Ye, X. Xu, J. Fang and X. Wang, Chem. Commun., 2014, 50, 7180-7183.

2. J. G. Hardy, A. R. Hirst, D. K. Smith, C. Brennan and I. Ashworth, Chem. Commun., 2005, 385-387.